arXiv:1703.06046v1 [cond-mat.mes-hall] 17 Mar 2017

Dynamic nuclear spin polarization in self-assembled quantum dots under zero magnetic field

R. Matsusaki,[1] R. Kaji,[1,*] S. Yamamoto,[1] H. Sasakura,[1] and S. Adachi[1,†]

[1]*Division of Applied Physics, Hokkaido University, N13 W8, Kitaku, Sapporo 060-8628, Japan*

(Dated: March 20, 2017)

We studied the zero-field dynamic nuclear spin polarization in a single $In_{0.75}Al_{0.25}As/Al_{0.3}Ga_{0.7}As$ quantum dot. Even without any external magnetic field, the positive trion excited by the circularly-polarized light generated an Overhauser field of up to ∼0.8 T. From the excitation power dependences of the Overhauser field and degree of circular polarization of the photoluminescence spectra, the relation between the Overhauser field and Knight field under zero external magnetic field was revealed clearly. In addition, we found that the nuclear depolarization rate decreased as the magnitude of the longitudinal magnetic field increased, which seemed to be caused by the influence of the quadrupolar interaction of nuclear spins. Further, the key parameters describing the dynamics of a coupled electron-nuclear spin system, the electron g-factor and the fluctuation of the Overhauser field, were evaluated in a typical single InAlAs quantum dot.

PACS numbers: 73.21.La, 78.67.Hc, 71.35.Pq, 71.70.Jp

I. INTRODUCTION

The carrier spin dynamics in low-dimensional semiconductor structures has attracted considerable interest because of the possibilities of spin storage and manipulation in future semiconductor electro-optic devices and quantum information processing[1–5]. This is because the confined carrier spins are relatively well decoupled from the orbital and charge degrees of freedom and the spin coherence is not obstructed by the commonly noted charge decoherence mechanisms[6]. For these potential applications, a complete understanding of the fundamental interactions among the spins in the localization volume is crucial as these interactions may limit the application performance because of the resultant spin decoherence. Hyperfine interaction (HFI), which is the magnetic interaction between the confined carrier spins and lattice nuclei, becomes especially important.

Because the lattice nuclei act as a reservoir for an optically or electrically injected electron spin, the *engineering of nuclear spins* such as the optical manipulation of the nuclear spin polarization (NSP) not only leads to the potential applications but also opens up a new spin physics. Along this line, the dynamic nuclear spin polarization (DNSP) induced by the electron-nucleus flip-flop part (e-n FF) of HFI and the resulting Overhauser field have been investigated intensively in semiconductor quantum dots (QDs)[7–11]. Because of the strong localization of the carrier wave function in a QD, the role of HFI in spin dynamics is drastically enhanced compared with those in bulks and quantum wells. One of the direct consequences of this enhanced HFI is a severe relaxation of electron spin polarization caused by a fluctuation of the Overhauser field in QDs[2,12,13]. Similarly, the fluctuation of the Knight field, which is the electron-generated effective magnetic field seen by each nucleus, induces the nuclear spin relaxation[14]. Interestingly, both effective fields also help to stabilize the spin counterpart under some conditions. Such a reciprocal influence makes the spin physics in nanostructures complicated and interesting. Until now, many fascinating and remarkable works have been reported: the bistability of the nuclear spin system[15–18], locking of the QD transition energy to the excitation laser[19–21], optically detected nuclear magnetic resonance (NMR) and spin echo for a single QD[22–24], and so on.

In contrast to those studies performed under large external magnetic fields, experimental reports under zero magnetic field have so far been insufficient[25–29]. As shown later, excitation by a circularly polarized beam induces a considerable Overhauser field under a wide range of experimental conditions, even if one does not intend to induce an Overhauser field. Thus, the understanding of HFI is necessary to analyze the experimental results performed under zero external magnetic field. In addition, zero-field DNSP reveals valuable information about the nuclear quadrupolar effect, which has been recently of interest from the viewpoint of stabilizing the NSP under zero field[30,31] and revealing the novel spin dynamics related to noncollinear HFI[21,32].

In this work, we study zero-field DNSP in a single InAlAs QD by focusing on the photoluminescence (PL) spectra of a positive trion (X^+). The degree of circular polarization (DCP) of X^+-PL works as a direct measure of the average electron spin polarization $\langle S_z \rangle$. Even without any external magnetic field, the spin-selected electron with circularly polarized excitation induces a large Overhauser field ($\boldsymbol{B}_N$) up to ∼0.8 T. Field B_N is much larger than the measured fluctuation (∼40 mT) and contributes to increase DCP by stabilizing the electron spin. From the excitation power dependences of the Overhauser shift (OHS) and DCP of X^+-PL, the relation between the Overhauser and Knight fields under zero external magnetic field is discussed. In addition, the depolarization of NSP changes depending on the magnitude of a longitudinal magnetic field (0-1 T), and this allows us to estimate the strength of quadrupolar interaction.

This paper is organized as follows: The InAlAs QD sample and the standard setup for single QD spectroscopy used in this work are described in the next section. In Section III, in order to estimate $\boldsymbol{B}_{\rm N}$ from the observed OHS correctly, an evaluation of the electron g-factor, including the sign, is carried out. Further, the fluctuation of $\boldsymbol{B}_{\rm N}$ is estimated from the correlation between the observed electronic Zeeman splitting and X^+-DCP. In Section IV, the measurement apparatus is improved to allow simultaneous acquisition of σ^+ and σ^- components of the PL spectra in order to detect small OHS and DCP accurately. In Section V, the zero-field DNSP is studied in detail via the excitation power dependences of the OHS and DCP using the improved setup. In addition, the impact of the nuclear quadrupolar effect on DNSP is studied from the dependence of the nuclear depolarization rate on the applied longitudinal magnetic field. Finally, the conclusion of this work is given in Section VI.

II. SAMPLE AND EXPERIMENTAL SETUP

Self-assembled $In_{0.75}Al_{0.25}As/Al_{0.3}Ga_{0.7}As$ QDs grown on an undoped (100)-GaAs substrate by molecular beam epitaxy were used in this work[8,33,34]. The average diameter, height, and density of the QDs were found to be ∼20 nm, ∼4 nm, and ∼5×10^{10} cm^{-2}, respectively, by the atomic force microscopy measurements of a reference uncapped QD layer. Assuming a lens-shaped QD based on the cross-section transmission electron microscope observation, the number of nuclei in a single QD is estimated to be roughly $N\sim3\times10^4$. After the fabrication of small mesa structures (top lateral diameter ∼150 nm), the micro-PL measurements in the time-integrated mode were performed at 6 K under longitudinal magnetic fields (B_z) up to 5 T.

A continuous wave Ti:sapphire laser was tuned to ∼730 nm to provide the transition energy to the foot of the wetting layer of the QDs. The laser beam was focused on the sample surface using a microscope objective lens (M Plan Apo NIR ×20, NA∼0.4). The QD emissions were collected by the same objective lens and were detected by a triple-grating spectrometer (Horiba Jobin-Yvon T64000, 1200 grooves/mm×3) and a liquid N_2-cooled Si-CCD detector (Princeton Instruments Spec-10:100BR). The spectral resolution that determines the PL energies was ∼5 μeV using the spectral fitting.

Figure 1(a) shows typical PL spectra obtained from a target single InAlAs QD at 6 K and 0 T. The PL signals were resolved to linearly polarized components (π^x, π^y). The spectra indicate the exciton family's emissions of this QD: the neutral biexciton (XX^0), neutral exciton (X^0), and positive trion (X^+) from the low energy side. Each charge state could be assigned by considering the fine structure splitting (FSS) and the binding energy. In this figure, the FSS of ∼73 μeV, the inverse pattern of FSS in the X^0 and XX^0 peaks, and no splitting in the X^+ peak are observed clearly.

Hereafter throughout this work, we focus on X^+-PL, which shows the largest peak in this QD. The ground state of X^+ consists of a spin-singlet formed of two holes and one electron, and thus, the emission polarization is essentially determined only by the electron spin. In this paper, the DCP is given by $\rho_{\rm c} = (I^- - I^+)/(I^- + I^+)$, where $I^{-(+)}$ is the PL intensity of $\sigma^{-(+)}$ component. Consequently, a high (low) value of the DCP indicates a large (small) degree of electron spin polarization $\langle S_{\rm z}\rangle$ according to $\langle S_{\rm z}\rangle = \rho_{\rm c}/2$, and the change in X^+-DCP can be used as a direct measure of $\langle S_{\rm z}\rangle$.

III. EVALUATIONS OF THE ELECTRON G-FACTOR AND FLUCTUATION OF THE OVERHAUSER FIELD

In this section, the key parameters describing the coupled electron-nuclear spin system, electron g-factor ($g_{\rm z}^{\rm e}$), and fluctuation of the Overhauser field ($\Delta B_{\rm N}$), are evaluated from the magneto-PLs under longitudinal magnetic fields $\boldsymbol{B}_{\rm z}$.

First, an individual evaluation of the electron and hole g-factors in the z-direction ($g_z^{\rm e}$, $g_z^{\rm h}$) is performed. This procedure is necessary for evaluating $\boldsymbol{B}_{\rm N}$ from the observed OHS, which is the energy shift of electron spin state induced by $\boldsymbol{B}_{\rm N}$. The method described below is based on the cancellation of $\boldsymbol{B}_z$ using $\boldsymbol{B}_{\rm N}$ on the electron spins.[35]

The Hamiltonian of HFI between an electron spin $\hat{\boldsymbol{S}}$ and N-lattice nuclear spins $\hat{\boldsymbol{I}}$ can be written as

$$\mathcal{H}_{\rm HF} = \frac{\nu_0}{2}\sum_j^N A^j|\varphi(\boldsymbol{r}_j)|^2\left[2\hat{I}_z^j\hat{S}_z + \left(\hat{I}_+^j\hat{S}_- + \hat{I}_-^j\hat{S}_+\right)\right], \tag{1}$$

where ν_0 is the two-atom cell volume, $\boldsymbol{r}_j$ is the position of the j-th nucleus with spin $\hat{I}^j$, $\varphi(\boldsymbol{r}_j)$ is the normalized electron envelope function, and A^j is the coupling constant of HFI[36]. Because a single electron interacts simultaneously with a large number of nuclei, the electron spin experiences an effective magnetic field originated from a mean NSP $\langle\hat{\boldsymbol{I}}^j\rangle$ expressed as,

$$\boldsymbol{B}_{\rm N} = \frac{\nu_0}{g^{\rm e}\mu_{\rm B}}\sum_j^N A^j|\varphi(\boldsymbol{r}_j)|^2\langle\hat{\boldsymbol{I}}^j\rangle, \tag{2}$$

where $\mu_{\rm B}$ is the Bohr magneton (∼58 μeV/T). Since the HFI on hole spin is usually negligible because of the small coupling constant[37–39], the Zeeman splitting of X^+-PL under $\boldsymbol{B}_{\rm z}$ is given as $\Delta E_{\rm Z} = g_z^{\rm h}\mu_{\rm B}|\boldsymbol{B}_{\rm z}| + g_{\rm z}^{\rm e}\mu_{\rm B}|\boldsymbol{B}_{\rm z} + \boldsymbol{B}_{\rm N}|$.

The left panel of Fig. 1(b) is a density plot of the Zeeman split X^+-PL under σ^- excitation with increasing $B_{\rm z}$. As clearly shown, the $\Delta E_{\rm Z}$ of X^+-PL decreases abruptly at the critical magnetic field $B_{\rm z}^{\rm HC}$(=4.5515 T). The direction of $\boldsymbol{B}_{\rm N}$ generated with σ^- excitation is opposite to that of $\boldsymbol{B}_{\rm z}$ ($\boldsymbol{B}_{\rm N}\cdot\boldsymbol{B}_{\rm z} < 0$). In this situation, the energy mismatch in the e-n FF process is relaxed, and the

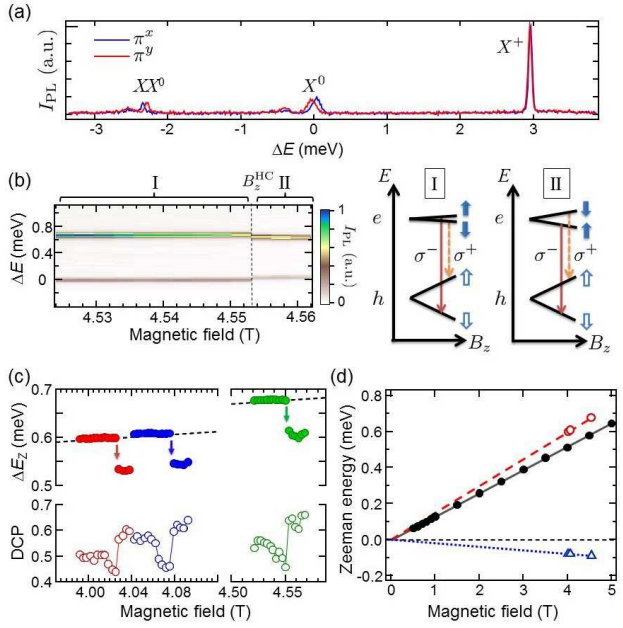

FIG. 1: (color online) (a) Polarization-resolved PL spectra of a target InAlAs QD at 6 K and 0 T. The horizontal axis is replotted from the midpoint of the X^0 doublet. (b) (left panel) Density plot of X^+-PL as a function of increasing B_z. The energy axis is replotted from the lower PL peak. (right panel) Level diagrams of the hole (open arrows) and the electron spins (solid arrows) in the smaller (larger) B_z than $B_z^{\rm HC}$, labeled as region I (II). (c) The observed $\Delta E_{\rm Z}$ near three different $B_z^{\rm HC}$. The dashed line is the calculated hole Zeeman splitting. In the lower panel, X^+-DCP is plotted. (d) Observed Zeeman energies of exciton (solid circles), electron (triangles), and hole states (open circles) and the fitting lines.

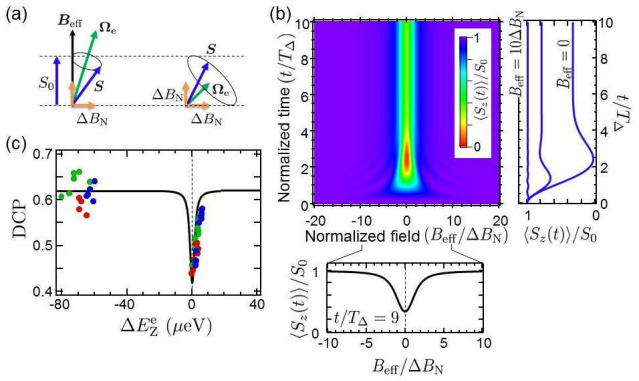

FIG. 2: (color online) (a) Schematics of electron spin precession around torque vector $\boldsymbol{\Omega}_{\rm e}$, which includes $\boldsymbol{B}_{\rm eff}$ and $\Delta\boldsymbol{B}_{\rm N}$. (b) Calculation of $\langle S_{\rm z}(t)\rangle/S_0$ as functions of normalized time (t/T_Δ) and magnetic field ($B_{\rm eff}/\Delta B_{\rm N}$). The vertical profiles at $B_{\rm eff}/\Delta B_{\rm N}$= 0, 2, 10 are indicated in the right panel, and the horizontal profile at t/T_Δ=9 is in the lower panel. (c) Experimentally obtained X^+-DCP as a function of $\Delta E_{\rm Z}^{\rm e}$. The solid curve is the calculation obtained using Eq. (3) with $\tau_{\rm r}$=0.75 ns and S_0=0.62, which includes the calculation of Fig. 2(b) with T_Δ=0.8 ns.

bistable behavior accompanied by the abrupt change in $B_{\rm N}$ appears. The right panel of Fig. 1(b) depicts the Zeeman levels of the electron and hole states in smaller (larger) $B_{\rm z}$ than $B_{\rm z}^{\rm HC}$, labeled as region I (II). While the electronic Zeeman splitting $\Delta E_{\rm Z}^{\rm e}$ is almost zero in region I, it is revived in region II. This change in $\Delta E_{\rm Z}^{\rm e}$ induces the abrupt decrease in $\Delta E_{\rm Z}$ if $g_{\rm z}^{\rm e}$ has the opposite sign to $g_{\rm z}^{\rm h}$. Note that $\Delta E_{\rm Z}^{\rm e}$ at $B_{\rm z}=B_{\rm z}^{\rm HC}$ is exactly zero because of the full compensation of $\boldsymbol{B}_{\rm z}$ by $\boldsymbol{B}_{\rm N}$. Thus, the observed $\Delta E_{\rm Z}$ at $B_{\rm z}^{\rm HC}$ corresponds to the hole Zeeman splitting, and the hole g-factor can be derived as $g_{\rm z}^{\rm h}=\Delta E_{\rm Z}(B_{\rm z}^{\rm HC})/\mu_{\rm B}B_{\rm z}^{\rm HC}$.

Figure 1(c) shows $\Delta E_{\rm Z}$ in the vicinity of three different values of $B_{\rm z}^{\rm HC}$, which can be obtained by changing the excitation power. The increase in the data points of $\Delta E_{\rm Z}(B_{\rm z}^{\rm HC})$ helps us to improve the accuracy for determining ($g_{\rm z}^{\rm h}$, $g_{\rm z}^{\rm e}$). Comparing $g_{\rm z}^{\rm h}$ to the exciton g-factor $g_{\rm z}^{\rm X}$ ($=g_{\rm z}^{\rm h}+g_{\rm z}^{\rm e}$) that can be obtained with linearly polarized excitation (i.e., $B_{\rm N}=0$), the electron g-factor can also be accessed. Note that the X^+-DCP changes depicted in the lower panel are synchronized with the changes in $\Delta E_{\rm Z}$ (that is, the changes in $B_{\rm N}$). This observation can be described by the effect of $\Delta B_{\rm N}$, as discussed later.

Figure 1(d) shows the Zeeman splittings of the exciton, hole, and electron spins as a function of $B_{\rm z}$. From the linear fittings, the g-factors of exciton, hole, and electron spins in this QD were evaluated as $g_{\rm z}^{\rm X}=2.23\pm0.01$, $g_{\rm z}^{\rm h}=2.57\pm0.01$, and $g_{\rm z}^{\rm e}=-0.34\pm0.02$, respectively. These values are close to those reported in previous work[35].

Next, we estimate the random fluctuation of the Overhauser field ($\Delta B_{\rm N}$) and the resultant electron spin dephasing time (T_Δ). According to the standard picture of spin relaxation, electron spin $\boldsymbol{S}$ precesses around the effective magnetic field and loses its coherence via scattering processes. Here, torque vector $\boldsymbol{\Omega}_{\rm e}$ is composed of macroscopic field $\boldsymbol{B}_{\rm eff}$ ($=\boldsymbol{B}_{\rm z}+\boldsymbol{B}_{\rm N}$) and fluctuating field $\Delta\boldsymbol{B}_{\rm N}$. In the absence of $\boldsymbol{B}_{\rm eff}$, $\boldsymbol{S}$ in a QD precesses coherently around $\Delta\boldsymbol{B}_{\rm N}$ during its lifetime, which is limited by recombination time $\tau_{\rm r}$. However, electron spin polarization $\langle S_{\rm z}\rangle$, which is an ensemble average over a large number of measurements, decreases within a characteristic time T_Δ due to the random distributions of the direction and magnitude of $\Delta\boldsymbol{B}_{\rm N}$, and it converges to $S_0/3$ (S_0: the initial value of $\langle S_{\rm z}\rangle$) over the long time limit (*frozen fluctuation model*)[12]. If a large $\boldsymbol{B}_{\rm eff}$ ($\gg\Delta\boldsymbol{B}_{\rm N}$) appears and $\boldsymbol{\Omega}_{\rm e}$ is nearly along the z-axis, the reduction of $\langle S_{\rm z}(t)\rangle$ is strongly suppressed, as shown in Fig. 2(a).

Figure 2(b) is $\langle S_{\rm z}(t)\rangle/S_0$, calculated as functions of normalized magnetic field $B_{\rm eff}/\Delta B_{\rm N}$ and normalized time t/T_Δ. The right panel shows the vertical profiles of the figure, which indicates clearly that the increase in $B_{\rm eff}$ suppresses the oscillation and reduction of $\langle S_{\rm z}(t)\rangle/S_0$. On the other hand, the lower panel is a horizontal plot at $t/T_\Delta=9$. In this long time region, the normalized electron spin polarization shows a dip structure centered

at the point of zero-$\boldsymbol{B}_{\rm eff}$, and its width is determined by $\Delta B_{\rm N}$.

The experimentally obtained DCP is determined by $\langle S_{\rm z}(t)\rangle$ and $\tau_{\rm r}$ ($\sim$0.75 ns), which is evaluated from other independent measurements. Assuming that the orientation of $\Delta\boldsymbol{B}_{\rm N}$ is randomly distributed over the accumulation time of the CCD detector (1 s), the DCP of time-integrated X^+-PL is given by

$$\rho_{\rm c} = \frac{2}{\tau_{\rm r}}\int \langle S_z(t)\rangle \exp(-t/\tau_{\rm r})dt. \qquad (3)$$

Note that this equation leads to a dip structure similar to the one in the lower panel of Fig. 2(b), and its width is determined by the ratio of T_Δ to $\tau_{\rm r}$.

Figure 2(c) shows the X^+-DCP as a function of $\Delta E_{\rm Z}^{\rm e}$ obtained from the data set in Fig. 1(c). The absence of data points around $\Delta E_{\rm Z}^{\rm e}$=-50-0 μeV is attributed to the abrupt changes in $\boldsymbol{B}_{\rm N}$ and DCP. The most important feature is that the observed X^+-DCP has a dip structure centered at point $\Delta E_{\rm Z}^{\rm e}$ $\sim$0, and it agrees well with the above explanation. By comparing it with the solid curve, which is obtained by Eq. (3) including the calculated results of Fig. 2(b), we can deduce the values $S_0 = 0.62$ and $T_\Delta = 0.8$ ns.

The magnitude of $\Delta\boldsymbol{B}_{\rm N}$ is estimated as $\Delta B_{\rm N}$=40 mT from the relation $\Delta B_{\rm N} = \hbar/(g^{\rm e}\mu_{\rm B}T_\Delta)$, assuming an isotropic electron g-factor. This value is comparable to those in InAs QDs ($\sim$30 mT)[40,41], InGaAs QDs ($\sim$10.5 mT)[42], and InP QDs ($\sim$15 mT)[43], and it coincides with the one in a different InAlAs QD[44]. Further, the validity of the observed $\Delta B_{\rm N}$ can be confirmed using the QD parameters ($g^{\rm e}$, $\tilde{A}$, $\tilde{I}$, N), where $\tilde{A}$ ($\tilde{I}$) is the average of A^j (I^j). From the relation $\Delta B_{\rm N} \cong \tilde{A}\tilde{I}/\sqrt{N}g^{\rm e}\mu_{\rm B}$ with the values ($g^{\rm e}$, $\tilde{A}$, $\tilde{I}$, N) = (-0.34, 52.6 μeV, 2.75, 3×10^4) for our $In_{0.75}Al_{0.25}As$ QD, $\Delta B_{\rm N}$ is roughly estimated as $\sim$42 mT, which agrees quite well with our observation.

IV. EXPERIMENTAL IMPROVEMENT FOR DCP MEASUREMENT

Under zero magnetic field, the energy splitting of X^+-PL is usually less than (or comparable with) the spectral width of QD transitions, and thus, the evaluations of OHS and DCP need to acquire the spectra with (σ^+, σ^-) components separately. Because this standard method is accompanied by more than one (at least two) PL acquisition procedure, the resultant OHS and DCP may be affected by some unfavorable effects such as variation in the excitation density and fluctuation of the sample temperature in the measurement intervals.

In order to reduce the measurement errors of OHS and DCP, we improved the experimental setup, as shown in Fig. 3; this enables the simultaneous acquisition of (σ^+, σ^-) components. The (σ^+, σ^-) PL components are converted to (π^x, π^y) ones by a quarter-wave plate (QWP), and they are displaced spatially from each other by a beam displacer, which serves as a linear polarizer in a

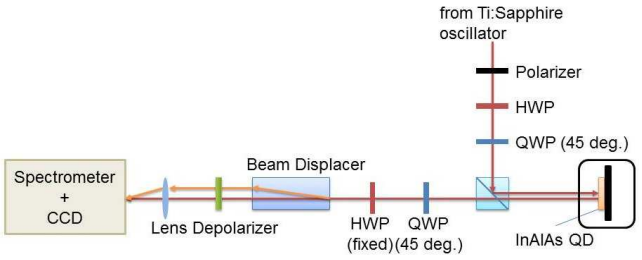

FIG. 3: (color online) Experimental setup for the fully simultaneous acquisition of σ^+ and σ^- components of the PL spectra for accurate OHS and DCP evaluation.

standard DCP measurement. Each displaced PL component is focused on a different detection area of the CCD array. Therefore, the OHS and DCP of the PL can be acquired by a single exposure process. The depolarizer after the beam displacer removes the polarization dependence of the grating diffraction efficiency in the spectrometer. The half-wave plates (HWPs) in the excitation and detection paths are used to compensate for the phase distortion of the circular polarization by many optical elements. Further, in order to avoid the unfavorable effects due to residual magnetization, the He-flow cryostat, which includes the InAlAs QD sample, was replaced apart from the superconducting magnet.

V. ZERO-FIELD DNSP AND IMPACT OF THE QUADRUPOLAR EFFECT

In a very low magnetic field, the expression of $\boldsymbol{B}_{\rm N}$ is obtained by considering the energy flow and nuclear spin temperature[14,36], and it can be expressed as

$$\boldsymbol{B}_{\rm N} = b_{\rm n}\frac{\boldsymbol{B}(\boldsymbol{B}\cdot\boldsymbol{S})}{|\boldsymbol{B}|^2+\xi B_{\rm L}^2}, \qquad (4)$$

where $b_{\rm n}$ is a proportionality constant, ξ is a coefficient close to unity, and $B_{\rm L}$ ($\sim$0.15 mT for bulk GaAs[45]) is a small local field due to the dipole-dipole interaction in the nuclear spin ensemble. According to Eq. (4), $B_{\rm N}$ cannot be produced without a non-zero magnetic field along $\boldsymbol{S}$. In general, the DNSP process is performed under an external magnetic field $B_{\rm z}$ that is larger than $B_{\rm L}$, where B_z suppresses the nuclear spin relaxation induced by $B_{\rm L}$. However, the strong localization of electron spin and resultant enhancement of HFI in a QD permit us to produce large $B_{\rm N}$, even under zero-$B_{\rm z}$.

Figure 4(a) shows the X^+-PL under σ^- excitation at $B_{\rm z} = 0$. The spectra were obtained with the setup described in Section IV. The sharp spectra in the figure indicate the full width at half maximum (FWHM) of $\sim$40 μeV and an OHS of 15 μeV. This OHS corresponds to $B_{\rm N}$=760 mT using the obtained value $g_{\rm z}^{\rm e} = -0.34$. In addition, the DCP is evaluated as $\sim$60%, which is

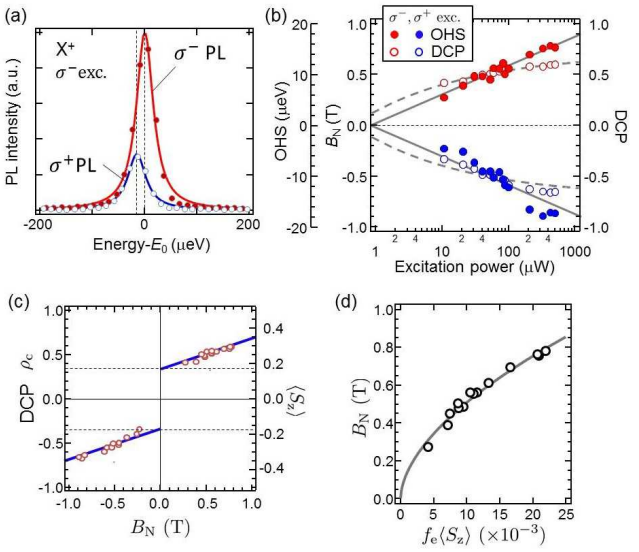

FIG. 4: (color online) (a) σ^+ and σ^- components of X^+-PL spectra under σ^--excitation at 0 T. For clarity, the spectra are shifted by energy E_0=1.6411 eV. An OHS of ∼15 μeV is observed. (b) Excitation power dependences of OHS ($\propto B_{\rm N}$) (solid circles) and DCP (open circles). (c) The measured DCP ($=2\langle S_z\rangle$) is plotted as a function of $B_{\rm N}$. (d) Obtained relation between $B_{\rm N}$ and $f_{\rm e}\langle S_{\rm z}\rangle$, which corresponds to the relation between $B_{\rm N}$ and $B_{\rm K}$.

larger than the value expected from the *frozen fluctuation model*, as discussed in Section III. The reason for the high DCP here is the presence of a large $B_{\rm N}$, which is sufficient to suppress the electron spin relaxation by $\Delta B_{\rm N}$ (∼40 mT) and stabilize $\langle S_z\rangle$. This large $B_{\rm N}$ under zero external magnetic field can be formed via nuclear spin cooling by the Knight field[14,25].

Because HFI is reciprocal between the electron and nuclear spin systems, the nuclei are also affected by an effective magnetic field $\boldsymbol{B}_{\rm K}$ (Knight field) induced by the average electron-spin polarization $\langle\hat{\boldsymbol{S}}\rangle$. The time-averaged Knight field acting on one specific nucleus j is given by

$$\boldsymbol{B}_{\rm K}^{j} = f_{\rm e}\frac{\nu_0 A^j}{g_{\rm N}\mu_{\rm N}}|\varphi(\boldsymbol{r}_j)|^2\langle\hat{\boldsymbol{S}}\rangle = f_{\rm e}b_{\rm e}^{j}\langle\hat{\boldsymbol{S}}\rangle, \qquad (5)$$

where $f_{\rm e}$ is a filling factor representing the occupation of a QD by an unpaired electron ($0 \le f_{\rm e} \le 1$), $g_{\rm N}$ is the nucleus g-factor, $\mu_{\rm N}$ is the nuclear magneton, and $b_{\rm e}^j$ is a proportionality constant. The Knight field can be tuned experimentally by changing excitation power $P_{\rm ex}$ and the polarization of the excitation light; the former affects $\boldsymbol{B}_{\rm K}$ through the change in $f_{\rm e}$, and the latter does so through the change in $\langle\hat{\boldsymbol{S}}\rangle$.

In order to investigate the role of $\boldsymbol{B}_{\rm K}$ in the process of nuclear spin cooling, we measured the $P_{\rm ex}$-dependences of OHS and DCP, as shown in Fig. 4(b). A slight asymmetry between σ^- and σ^+ excitations may be caused by the variation of the excitation power. The OHS increases almost linearly on $\log(P_{\rm ex})$ in the experimental region of $P_{\rm ex}$, while the corresponding DCP saturates at 60% in the high-$P_{\rm ex}$ region. The change in DCP is due to the stabilization of $\langle S_{\rm z}\rangle$ by $\boldsymbol{B}_{\rm N}$. To highlight this scenario, we plotted DCP versus $B_{\rm N}$ (Fig. 4(c)) using the data set of Fig. 4(b), where $|\rho_{\rm c}|$ increases almost linearly with $|\boldsymbol{B}_{\rm N}|$. Even at the minimum $P_{\rm ex}$ in this experiment, a $B_{\rm N}$ of ∼200 mT, which is larger than $\Delta B_{\rm N}$, is produced, and thus, an obvious reduction of DCP ($\rho_{\rm c} = 2\langle S_{\rm z}\rangle$) caused by $\Delta B_{\rm N}$ does not appear in the figure.

In the case of QDs where large nuclear fields are generated, the dependence of the e-n FF rate (hidden in $b_{\rm n}$ in Eq. (4)) on the total magnetic field $\boldsymbol{B} + \boldsymbol{B}_{\rm N}$ has to be taken into account. Thus, the expression for $\boldsymbol{B}_{\rm N}$ (Eq. (4)), is replaced by the steady state solutions of the following rate equation for $\langle I_{\rm z}\rangle$:

$$\frac{d\langle I_{\rm z}\rangle}{dt} = -\frac{1}{T_{\rm NF}}\left[\langle I_{\rm z}\rangle - \tilde{Q}\left(\langle S_{\rm z}\rangle - \langle S_{\rm z}\rangle_0\right)\right] - \frac{1}{T_{\rm ND}}\langle I_{\rm z}\rangle, \qquad (6)$$

where $\tilde{Q} = \sum_j I^j(I^j+1)/[NS(S+1)]$ is a numerical constant representing the angular momentum conversion and $\langle S_{\rm z}\rangle_0$ is the average electron spin polarization at thermal equilibrium. The first term on the right-hand side represents the DNSP formation driven by the non-equilibrium electron spin, and the second term accounts for the depolarization of nuclear spin system with time constant $T_{\rm ND}$. The DNSP formation rate $1/T_{\rm NF}$ is given as

$$\frac{1}{T_{\rm NF}} = 2f_{\rm e}\tau_{\rm c}\left(\frac{\tilde{A}}{N\hbar}\right)^2 \Big/ \left[1 + \left(\frac{\tau_{\rm c}}{\hbar}\right)^2 (g_{\rm z}^{\rm e}\mu_{\rm B}B_{\rm z} \pm \tilde{A}\langle I_{\rm z}\rangle)^2\right], \qquad (7)$$

where $\tau_{\rm c}$ is the correlation time of the hyperfine perturbation. Using Eqs. (6) and (7), $f_{\rm e}$ can be estimated from the fitting of the data in Fig. 4(b), and $f_{\rm e}$ was found to be proportional to $\log(P_{\rm ex})$ (not shown here).

In Fig. 4(d), $|\boldsymbol{B}_{\rm N}|$ is plotted as a function of the product of $f_{\rm e}$ and $\langle S_{\rm z}\rangle$. From Eq. (5), $f_{\rm e}\langle S_{\rm z}\rangle$ is considered to be proportional to the magnitude of $\boldsymbol{B}_{\rm K}$. Because the constant $b_{\rm e}$, which is the average of $b_{\rm e}^j$, of our QD is thought to be ∼40 mT, the magnitude of $B_{\rm K}$ is estimated to be $0.2-1.0$ mT in the experimental region of $P_{\rm ex}$; this effective field for the nucleus is larger than $B_{\rm L}$. Actually, Lai *et al.* evaluated $B_{\rm K} = \pm 0.6$ mT directly through the field compensation (i.e., $\boldsymbol{B}_{\rm K} + \boldsymbol{B}_{\rm z} = 0$) accompanied by the reduction of X^--DCP in InAs QDs under $\sigma^\pm$ excitation[25]. From the relation $g_{\rm e}\mu_{\rm B}\boldsymbol{B}_{\rm N}^{\rm max} = Ng_{\rm N}\mu_{\rm N}\boldsymbol{B}_{\rm K}^{\rm max}$, $|\boldsymbol{B}_{\rm K}^{\rm max}|$ is estimated to be a few tens of millitesla.

Finally, we study the role of the quadrupolar field and evaluate the magnitude experimentally. Figure 5(a) indicates the OHS as a function of the measured $\langle S_{\rm z}\rangle$ under the external magnetic fields $B_{\rm z} = 0$ and 0.8 T. The excitation power was fixed to 100 μW, and the polarization of the excitation light was changed systematically. While the change in OHS at 0 T is exactly antisymmetric with respect to the change in the sign of $\langle S_{\rm z}\rangle$, this is not the case at 0.8 T; the OHS in positive $\langle S_{\rm z}\rangle$ is larger than that in negative $\langle S_{\rm z}\rangle$, which is caused by the difference of the DNSP formation rate. Note that the application of $B_{\rm z}$

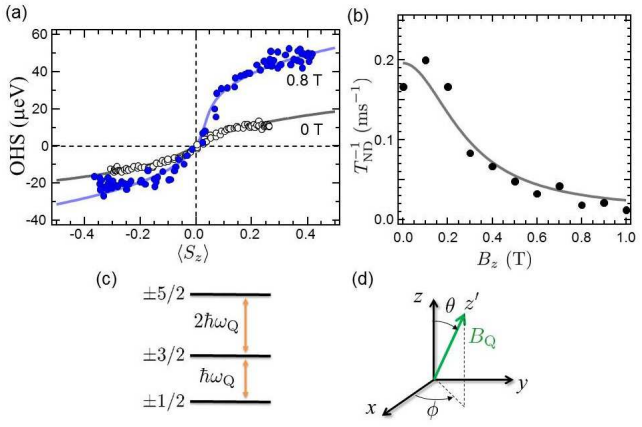

FIG. 5: (color online) (a) OHS as a function of $\langle S_z \rangle$ at B_z =0 T and 0.8 T (P_{exc}=100 μW). $\langle S_z \rangle$ is converted from the measured DCP from X^+ PL line intensity. Solid lines are the fitting curves using Eq. (6). (b) Dependence of nuclear spin relaxation rate T_{ND}^{-1} on longitudinal magnetic field B_z. (c) Energy level diagram at B_z=0 under the influence of QI for nuclear spin I=5/2. (d) Quadrupolar field B_Q is tilted by θ to the z axis.

leads to an increase in OHS even in the negative $\langle S_z \rangle$ region. This observation seems to be strange at first view because the generated $\boldsymbol{B}_N$ has the same direction with $\boldsymbol{B}_z$ in the negative $\langle S_z \rangle$ region. According to Eq. (7), $1/T_{NF}$ and the resultant OHS decrease if other parameters are unchanged.

Solid curves in the figure are the fittings obtained from Eq. (6) by changing $\langle S_z \rangle$, where the nuclear spin depolarization rate $1/T_{ND}$ is unique for each B_z. The best fittings show that T_{ND} = 6 and 56 ms for B_z=0 and 0.8 T, respectively. The result indicates that the application of B_z suppresses $1/T_{ND}$. We then investigated the B_z-dependence of $1/T_{ND}$ in detail by changing the magnitude of B_z up to 1 T while other experimental conditions were unchanged. Figure 5(b) depicts the deduced $1/T_{ND}$ as a function of B_z. As clearly shown, the nuclear depolarization rate decreases systematically with increasing B_z and approaches a saturated value.

The following two mechanisms may contribute to the nuclear depolarization term: the dipolar interaction between nuclear spins and the quadrupolar interaction (QI). It is widely accepted that the dipolar interaction is responsible not only for a fast depolarization in a very low magnetic field ($\leq B_L$) but also for a slow depolarization through the nuclear spin diffusion process[46]. Although the nuclear spin diffusion process is effective even under a large B_z, the efficiency of this depolarization mechanism does not depend on the magnitude of B_z. Therefore, the observed change in $1/T_{ND}$ seems to originate from the QI mechanism.

The QI originates from the coupling between an electric quadrupolar moment of nuclear spin ($I > 1/2$) and an inhomogeneous electric field gradient (EFG) caused by the alloy disorder and/or the local strain in the crystal, and it splits the $(2I + 1)$ spin levels according to the square of their angular momentum projection, as depicted in Fig. 5(c). Here, the splitting energy is characterized by the term $\hbar\omega_Q$, which is proportional to the nuclear quadrupolar moment and the EFG.

For the purpose of quantitative comparison, we introduce an effective magnetic field by the QI, $B_Q \equiv \hbar\omega_Q/g_N\mu_N$. Further, the EFG in a QD is assumed to have cylindrical symmetry with respect to the z-axis, as shown in Fig. 5(d) for simplicity. The influences of QI in the self-assembled QDs are thought to be large compared to those in unstrained systems because of a large residual strain associated with the QD formation process, and the estimated value of B_Q is in about the 100 mT range. This effective field, originated from QI, suppresses the dipolar coupling and resultant nuclear depolarization process effectively.

The EFG should orient almost along the $z-$axis, which has been confirmed experimentally in In(Ga)As QDs by single-QD NMR[22,23]. However, if the EFG axis is tilted by an angle θ, the QI may be responsible for a specific mechanism of nuclear spin depolarization. Under this condition, one nuclear state $|I_z\rangle$ couples with the other states $|I_z \pm 1\rangle$, and thus the differences in the populations of these states and resultant polarizations are partially canceled out. Further, a QI with non-zero θ may also contribute to $1/T_{ND}$ by coupling with the temporal fluctuation of the longitudinal part of HFI (i.e., $\propto S_z I_z$) as suggested by Huang *et al*[32]. This type of depolarization seems to be suppressed by applying a longitudinal magnetic field because B_z, which is comparable or larger than B_Q, can restore the eigenaxis of nuclear spin along z and decouple between $|I_z\rangle$ and $|I_z \pm 1\rangle$.

From these considerations, the nuclear depolarization rate can be assumed as follows[11,41]:

$$T_{ND}^{-1} = T_{ND\infty}^{-1} + T_{ND0}^{-1}\left[1 + \left(\frac{B_z}{B'_Q}\right)^2\right]^{-1}, \qquad (8)$$

where $1/T_{ND\infty}$ is a constant term representing the depolarization rate at the high-B_z limit, $1/T_{ND0}$ is an amplitude of the Lorentzian part describing qualitatively the slowdown of $1/T_{ND}$ at high-B_z, and B'_Q is a measure of the quadrupolar field. The solid curve in Fig. 5(b) is a fitting obtained using Eq. (8), and it reproduces the experimental result quite well. From the fitting, $T_{ND\infty}$ = 100 ms, T_{ND0} = 5 ms, and B'_Q = 280 mT were obtained. The obtained value of B'_Q is comparable with those evaluated in self-assembled In(Ga)As/GaAs QDs (∼400 mT[41] and ∼300 mT[47]).

When a QD does not include any charge carriers, the dipolar interaction between nuclear spins plays a dominant role in the decay of NSP. In particular, the nuclear spin diffusion is still effective even under a large B_z, and thus, it induces a severe problem related to the *nuclear spin bath noise*. Along this line, the quadrupolar

interaction has a positive effect thanks to the resultant non-equivalent energy spacing of nuclear spin levels; it inhibits the simultaneous spin flip between nuclear spins due to the energy mismatch. In contrast, the quadrupolar interaction can induce a specific mechanism of nuclear spin depolarization if the QD is occupied with an electron spin and the principal axis of EFG is away from the z-axis, as discussed above. These properties make QI more important and interesting for understanding the coupled electron-nuclear spin system deeply, and thus, our observation will serve as useful information.

VI. CONCLUSION

We investigated the DNSP in a self-assembled InAlAs quantum dot under a zero external magnetic field by focusing on the PL from the positive trion X^+. The DCP of X^+-PL works as a direct measure of the average electron spin polarization $\langle S_z \rangle$. First, the key parameters describing the coupled electron-nuclear spin system, electron g-factor and fluctuation of the Overhauser field of a target single QD were evaluated experimentally. After the experimental setup was improved to enable highly accurate evaluations of OHS and DCP, the zero-field DNSP was studied in detail. The spin-selectively-excited electron generated considerable Overhauser fields of up to $\sim$0.8 T. From the excitation power dependences of OHS and DCP, the relation between the generated Overhauser field and generating Knight field at 0 T was clearly obtained. The resulting comprehensive knowledge about zero-field DNSP, including the evaluations of key parameters for a typical self-assembled QD, will serve as useful information.

Further, we found a gradual reduction by almost one-order of the nuclear depolarization rate $T_{\rm ND}^{-1}$ by increasing the longitudinal magnetic field up to 1 T. The change in $T_{\rm ND}^{-1}$ seemed to be related to the quadrupolar interaction with the tilted principal axis, and this observation can be interpreted as the restoring of the eigenaxis of nuclear spin. We believe that this observation in zero-field DNSP has not been previously reported and can contribute to the engineering of nuclear spins in QDs.

This work was supported in part by JSPS KAKENHI (Grants No. 25247047 and No. 26800162).

* Electronic address: r-kaji@eng.hokudai.ac.jp
† Electronic address: adachi-s@eng.hokudai.ac.jp

[1] *Semiconductor Spintronics and Quantum Computation*, edited by D. D. Awschalom, D. Loss, and N. Samarth (Springer-Verlag, Berlin, 2002).
[2] *Spin Physics in Semiconductors*, Springer Series in Solid-State Sciences Vol. 157, Chaps. 1 and 11, edited by M. I. Dyakonov (Springer, Berlin, 2008).
[3] *Optical Generation and Control of Quantum Coherence in Semiconductor Nanostructures*, edited by G. Slavcheva and P. Roussignol (Springer-Verlag, Berlin, 2010).
[4] J. M. Taylor, C. M. Marcus, and M. D. Lukin, Phys. Rev. Lett. **90**, 206803 (2003).
[5] S. Muto, S. Adachi, T. Yokoi, H. Sasakura, and I. Suemune, Appl. Phys. Lett. **87**, 112506 (2005).
[6] A. V. Khaetskii and Y. V. Nazarov, Phys. Rev. B **61**, 12639 (2000).
[7] D. Gammon, Al. L. Efros, T. A. Kennedy, M. Rosen, D. S. Katzer, D. Park, S. W. Brown, V. L. Korenev, and I. A. Merkulov, Phys. Rev. Lett. **86**, 5176 (2001).
[8] T. Yokoi, S. Adachi, H. Sasakura, S. Muto, H. Z. Song, T. Usuki, and S. Hirose, Phys. Rev. B **71**, 041307(R) (2005).
[9] A. S. Bracker, E. A. Stinaff, D. Gammon, M. E. Ware, J. G. Tischler, A. Shabaev, Al. L. Efros, D. Park, D. Gershoni, V. L. Korenev, and I. A. Merkulov, Phys. Rev. Lett. **94**, 047402 (2005).
[10] B. Eble, O. Krebs, A. Lemaître, K. Kowalik, A. Kudelski, P. Voisin, B. Urbaszek, X. Marie, and T. Amand, Phys. Rev. B **74**, 081306(R) (2006).
[11] Recent optical investigation of nuclear spin physics in QDs are reviewed comprehensively: B. Urbaszek, X. Marie, T. Amand, O. Krebs, P. Voisin, P. Maletinsky, A. Högele, A. Imamoglu, Rev. Mod. Phys. **85**, 79 (2013).
[12] I. A. Merkulov, Al. L. Efros, and M. Rosen, Phys. Rev. B **65**, 205309 (2002).
[13] P.-F. Braun, X. Marie, L. Lombez, B. Urbaszek, T. Amand, P. Renucci, V. K. Kalevich, K.V. Kavokin, O. Krebs, P. Voisin, and Y. Masumoto, Phys. Rev. Lett. **94**, 116601 (2005).
[14] *Optical Orientation*, Modern Problems in Condensed Matter Sciences Vol. 8, Chaps. 2 and 5, edited by F.Meier and B. Zakharchenya (North-Holland, NewYork, 1984).
[15] P.-F. Braun, B. Urbaszek, T. Amand, X. Marie, O. Krebs, B. Eble, A. Lemaître, and P. Voisin, Phys. Rev. B **74**, 245306 (2006).
[16] A. I. Tartakovskii, T. Wright, A. Russell, A. B. Van'kov, J. Skiba-Szymanska, I. Drouzas, R. S. Kolodka, M. S. Skolnick, P. W. Fry, A. Tahraoui, H.-Y. Liu, and M. Hopkinson, Phys. Rev. Lett. **98**, 026806 (2007).
[17] P. Maletinsky, C. W. Lai, A. Badolato, and A. Imamoglu, Phys. Rev. B **75** 035409 (2007).
[18] R. Kaji, S. Adachi, H. Sasakura, and S. Muto, Phys. Rev. B **77**, 115345 (2008).
[19] C. Latta, A. Hogele, Y. Zhao, A. N. Vamivakas, P. Maletinsky, M. Kroner, J. Dreiser, I. Carusotto, A. Badolato, D. Schuh, W. Wegscheider, M. Atature, and A. Imamoglu, Nat. Phys. **5**, 758 (2009).
[20] X. Xu, W. Yao, B. Sun, D. G. Steel, A. S. Bracker, D. Gammon, and L. J. Sham, Nature **459**, 1105 (2009).
[21] A. Högele, M. Kroner, C. Latta, M. Claassen, I. Carusotto, C. Bulutay, and A. Imamoglu, Phys. Rev. Lett. **108**, 197403 (2012).
[22] E. A. Chekhovich, K. V. Kavokin, J. Puebla, A. B. Krysa, M. Hopkinson, A. D. Andreev, A. M. Sanchez, R. Beanland, M. S. Skolnick and A. I. Tartakovskii, Nat. Nanotech. **7**, 646 (2012).
[23] E. A. Chekhovich, M. Hopkinson, M. S. Skolnick, and A. I. Tartakovskii, Nat. Commun. **6**, 6348 (2015).

[24] R. Stockill, C. Le Gall, C. Matthiesen, L. Huthmacher, E. Clarke, M. Hugues, and M. Atatüre, Nat. Commun. **7**, 12745 (2016).

[25] C. W. Lai, P. Maletinsky, A. Badolato, and A. Imamoglue, Phys. Rev. Lett. **96**, 167403 (2006).

[26] R. Oulton, A. Greilich, S. Y. Verbin, R. V. Cherbunin, T. Auer, D. R. Yakovlev, M. Bayer, I. A. Merkulov, V. Stavarache, D. Reuter, and A. Wieck, Phys. Rev. Lett. **98**, 107401 (2007).

[27] T. Belhadj, C.-M. Simon, T. Amand, P. Renucci, B. Chatel, O. Krebs, A. Lemaître, P. Voisin, X. Marie, and B. Urbaszek, Phys. Rev. Lett. **103**, 086601 (2009).

[28] L. A. Larsson, E. S. Moskalenko, and P. O. Holtz, Appl. Phys. Lett. **98**, 071906 (2011).

[29] C. F. Fong, Y. Ota, E. Harbord, S. Iwamoto, and Y. Arakawa, Phys. Rev. B **93**, 125306 (2016).

[30] R. I. Dzhioev and V. L. Korenev, Phys. Rev. Lett. **99**, 037401 (2007).

[31] O. Krebs, P. Maletinsky, T. Amand, B. Urbaszek, A. Lemaître, P. Voisin, X. Marie, and A. Imamoglu, Phys. Rev. Lett. **104**, 056603 (2010).

[32] C.-W. Huang and X. Hu, Phys. Rev. B **81**, 205304 (2010).

[33] H. Sasakura, S. Adachi, S. Muto, H. Z. Song, T. Miyazawa, and Y. Nakata, Physica E (Amsterdam) **21**, 511 (2004).

[34] H. Sasakura, S. Adachi, S. Muto, H. Z. Song, T. Miyazawa, and T. Usuki, Jpn. J. Appl. Phys., Part 1 **43**, 2110 (2004).

[35] R. Kaji, S. Adachi, H. Sasakura, and S. Muto, Appl. Phys. Lett. **91**, 261904 (2007).

[36] *The Principle of Nuclear Magnetism*, A. Abragam (Oxford University Press, Oxford, UK, 1961).

[37] C. Testelin, F. Bernardot, B. Eble, and M. Chamarro, Phys. Rev. B **79**, 195440 (2009).

[38] B. Eble, C. Testelin, P. Desfonds, F. Bernardot, A. Balocchi, T. Amand, A. Miard, A. Lemaître, X. Marie, and M. Chamarro, Phys. Rev. Lett. **102**, 146601 (2009).

[39] R. Kaji, S. Ohno, T. Hozumi, and S. Adachi, J. Appl. Phys. **113**, 203511 (2013).

[40] O. Krebs, B. Eble, A. Lemaître, B. Urbaszek, K. Kowalik, A. Kudelski, X. Marie, T. Amand, and P. Voisin, Phys. Stat. Solidi. A **204**, 202 (2007).

[41] O. Krebs, B. Eble, A. Lemaître, P. Voisin, B. Urbaszek, T. Amand, and X. Marie, C. R. Phys. **9**, 874 (2008).

[42] A. Bechtold, D. Ranuch, F. Li, T. Simmet, P.-L. Ardelt, A. Regler, K. Muller, N. A. Sinitsyn, and J. J. Finley, Nat. Phys. **11**,1005 (2015).

[43] B. Pal, S. Y. Verbin, I. V. Ignatiev, M. Ikezawa, and Y. Masumoto, Phys. Rev. B **75**, 125322 (2007).

[44] R. Kaji, S. Adachi, H. Sasakura, and S. Muto, Phys. Rev. B **85**, 155315 (2012).

[45] D. Paget, G. Lampel, B. Sapoval, and V. I. Safarov, Phys. Rev. B **15**, 5780 (1977).

[46] S. Adachi, R. Kaji, S. Furukawa, Y. Yokoyama, and S. Muto, J. Appl. Phys. **111**, 103531 (2012).

[47] P. Maletinsky, M. Kroner, and A. Imamoglu, Nat. Phys. **5**, 407 (2009).